International Journal of Astrobiology 15 (1): 17–25 (2016)
doi:10.1017/S1473550415000348

Possible role of Prussian blue nanoparticles in chemical evolution: interaction with ribose nucleotides

Rachana Sharma, Md. Asif Iqubal and Kamaluddin

Department of Chemistry, Indian Institute of Technology Roorkee, Roorkee-247 667, Uttrakhand, India
e-mail: kamalfcy@iitr.ac.in; kamalfcy@gmail.com

Abstract: Ribonucleotides (RMPs) are the building blocks of genetic material consisting of a sugar group, a phosphate group and a nucleobase. Prussian blue (PB) is an ancient compound which is supposed to have formed under the conditions of primitive Earth. The interaction between nucleotides and mineral surfaces is of primary importance in the context of prebiotic chemistry. In the present work, the adsorption of RMPs on PB has been studied in the concentration range 0.4×10^{-4}–3.0×10^{-4} M of RMPs at pH 7.5, $T = 27°C$ and found to be 53.1, 41.7, 25.8 and 24.0% for adenosine 5′-monophosphate (5′-AMP), guanosine 5′-monophosphate, cytidine 5′-monophosphate and uridine 5′-monophosphate, respectively. Optimum conditions for the adsorption were studied as a function of concentration, time, amount of adsorbent and pH and data obtained were found to fit the Langmuir adsorption isotherm. Langmuir constants (K_L and X_m) values were calculated. Fourier transform infrared spectroscopy, Raman spectroscopy, field-emission scanning electron microscopy and X-ray diffractometry techniques were used to investigate the interaction of RMPs on PB surface. Adsorption kinetics of 5′-AMP on PB has been found to be pseudo-second order. Results obtained from this study should prove valuable for a better understanding of the mechanism of RMP–PB interaction.

Received 8 May 2015, accepted 27 July 2015, first published online 1 October 2015

Key words: Adsorption, FT-IR, FE-SEM, Prussian blue, ribonucleotides

Introduction

The first hypothesis regarding the problem of concentrating the biomolecules in the primitive sea was due to John Bernal in 1951. He suggested that minerals catalysed the formation of biomolecules by adsorbing monomers on the surface so that condensation reaction could easily occur. It was also suggested that mineral surfaces might also have shielded the adsorbed biomolecules from the destructive effects of ultraviolet (UV) radiations. Since then a large number of studies involving adsorption and polymerization of nucleic acid components on several materials have appeared. A survey shows that the interaction of nucleic acid components on clay surfaces (Ferris & Hagan 1986; Ferris *et al.* 1989; Franchi *et al.* 1999, 2003; Cai *et al.* 2006; Hashizume & Theng 2007; Hashizume *et al.* 2010), on metal oxides such as iron oxide–hydroxide polymorphs (Holm *et al.* 1993), haematite (Arora *et al.* 2007), ZnO (Arora & Kamaluddin 2007), alumina (Arora & Kamaluddin 2009), TiO_2 (Cleaves *et al.* 2010) and double-metal cyanide complexes also (Ali *et al.* 2004, 2007) have been studied. More recent works have reported the interaction of nucleic acid with clays (Carneiro *et al.* 2011; Sciascia *et al.* 2011; Bau *et al.* 2012; Feuillie *et al.* 2013), silica surfaces (Georgelin *et al.* 2013) and with double-metal cyanide complexes (Kumar & Kamaluddin 2013) too.

In the family of double-metal cyanide complexes Prussian blue (PB) is the earliest synthesized and has been used in industry, pharmaceutics and science. Its basic structure consists of alternating high-spin Fe(III) coordinated with 'N' atom and low-spin Fe(II) coordinated with 'C' atom of cyanide ligand in a face-centred cubic arrangement (Herren *et al.* 1980). For charge balance, a quarter of $[Fe^{II}(CN)_6]$ sites remain vacant and filled with water molecules located at empty nitrogen sites and coordinated with Fe^{III}.

Cyanide has been reported as a product in several simulated prebiotic experiments and is supposed to have been readily available under the primitive Earth conditions. HCN would be expected to react with Fe^{2+} present in comparative high concentration in the Archean hydrosphere (Keefe & Miller 1996). The formation of PB under the condition of the prebiotic Earth was suggested by Arrhenius *et al.* (1994). He proposed that iron (II) ion present in adequate quantity in primitive ocean would yield the insoluble salt on reaction with ferrocyanide ion on partial oxidation. The existence of PB under prebiotic condition has also been discussed by Bermejo *et al.* (2007). The existence and formation of PB in prebiotic oceans has also been described by Gibson *et al.* (2010). The possible reaction pathways of ribonucleotides (RMPs) have been based on the assumptions that they must have formed from their respective components, a nucleobase, ribose sugar and phosphate (Szostak 2009). Orthophosphate is the most common source of phosphate on the modern Earth today, but this was also likely the case on the prebiotic Earth. Possible sources of phosphorus in the form of ortho, meta and pyrophosphate for

nucleotide synthesis in the early Earth conditions could be due to volcanism (Yamagata *et al.* 1991). The traditional view for the prebiotic synthesis of nucleotides is to phosphorylate the appropriate nucleoside. The first attempt regarding this was tried by Lohrmann & Orgel (1971) who discovered that nucleosides can be phosphorylated. They did the phosphorylation of a nucleoside in a mixture containing urea, ammonium chloride, ammonium bicarbonate and sodium phosphate at 65–100°C. Recently, Powner *et al.* (2009) synthesized pyrimidine nucleotides by taking cyanamide, cyanoacetylene, glycolaldehyde, glyceraldehyde and inorganic phosphates as the plausible prebiotic starting material. Under the circumstances it appears relevant to investigate the interaction of nucleic acid components with PB to better understand the mechanism and kinetics of adsorption. In the present work, we aim to study in detail the adsorption of four RMPs on the surface of PB. The adsorption kinetics of adenosine 5′-monophosphate (5′-AMP) has also been investigated.

Experimental procedure

Materials and methods

Potassium hexacyanoferrate(II) ($K_4[Fe(CN)_6].6H_2O$ was purchased from E. Merck, iron(III) nitrate ($Fe(NO_3)_3{\cdot}9H_2O$) and RMPs from Sigma-Aldrich. The characteristic properties of RMPs are listed in Table S1 (supplementary information). The reagents were used without further purification. Distilled deionized (Millipore RO 10TS, 18 MΩ) water was used throughout the studies. Graphs are plotted and smoothened using Origin Pro 8.1 software. Adsorption studies were carried out at room temperature.

Nanosized PB was prepared by the previously reported procedure (Gotoh *et al.* 2007). In brief a solution of Fe $(NO_3)_3{\cdot}9H_2O$ (40.1 mmol in 30 ml of water) was added dropwise to a solution of $K_4[Fe(CN)_6].6H_2O$ (29.8 mmol in 60 ml of water) with constant stirring at room temperature. The resulting precipitate was filtered through a Buchner funnel and washed four times with 400 ml of water followed by washing with 80 ml of methanol. The precipitate was dried in an oven at about 80°C overnight. The solid material obtained was PB. It was crushed and sieved through a 150 mesh size sieve.

Elemental analysis of the synthesized PB was performed using an ElementarVario ELHI CHNS analyser and the percentage of iron was determined using an atomic absorption spectrophotometer (Perkin Elmer AAnalyst 800). TG/DTA analysis was carried out with an EXSTAR TG/DTA 6300 thermal analyser with a heating rate of 10°C min^{-1} in air using alumina as reference. Powder X-ray diffraction analysis of samples was carried out using a Brucker AXS D8 Advance X-ray diffractometer (XRD; Cu-Kα, λ = 0.1540 nm).

Ultraviolet–visible (UV–vis) absorption spectra of the samples were recorded in the wavelength range of 190–1100 nm with a resolution of 0.1 nm in a quartz cuvette using a Shimadzu UV-16001 spectrophotometer. The infrared spectra of samples were recorded using KBr pressed disc technique by a Fourier transform infrared spectrometer (FT-IR; Perkin-Elmer-1600 series), operating in the range of 400–4000 cm^{-1}. Spectra were recorded with a scanning speed of 2 mm s^{-1} and resolution of 2 cm^{-1}. Raman spectra of the samples were recorded using an inVia RENISHAW Raman spectrophotometer (serial no. 021R88) equipped with a confocal microscope (serial no. H33197) with 4 cm^{-1} resolution. An argon ion laser operating at 514.5 nm was used as excitation source.

Morphological studies of the samples were carried out using field-emission scanning electron microscopy (FE-SEM) and transmission electron microscopy (TEM) techniques. Surface morphology of the sample was observed by FEI Quanta 200F SEM operating at 20 kV. The sample was first made conducting by smearing the sample on a conducting carbon tape and then gold sputtered for 100 s in a high vacuum chamber. Elemental compositions of the samples were also determined using an energy-dispersive X-ray (EDX) analysis facility attached with the FE-SEM. TEM images of the PB nanoparticles were observed using FEI TECHNAI G20 transmission electron microscope operating at 200 kV. For the TEM analysis, a few mg of the sample powder was dispersed in acetone and sonicated for about 15 min. Then, a drop of the suspension was put on carbon-coated copper grid followed by drying in air.

The textural characteristics of samples were determined from a N_2 adsorption isotherms at 77 K using a Nova 2200e (Quantachrome) instrument. Prior to analysis, samples were heated at 150°C in vacuum for 2 h. Helium gas was used for dead space measurements. The BET (Brunauer, Emmet and Teller) equation was utilized to measure the specific surface area of porous solids (Brunauer *et al.* 1938).

$$\frac{P}{V(P_0 - P)} = \frac{1}{V_m C} + \frac{C-1}{V_m}\left(\frac{P}{P_0}\right)$$

where P/P_0 is relative pressure, V is the adsorbed gas quantity, V_m is the monolayer-adsorbed gas quantity and C is the BET constant. A linear plot of $P/V(P_0-P)$ versus P/P_0 was used to find out the value of surface area of samples from the slope and intercept.

Adsorption protocol

Batch adsorption experiments were performed to measure the adsorption of RMPs on the surface of PB. The effect of adsorbate concentration, contact time, amount of adsorbent and pH of the solution, necessary to establish the adsorption equilibria was studied. About 25 mg of PB were added into 5 ml of RMP solution (ranging from 0.4×10^{-4} to 3.0×10^{-4} M) in a 25 ml glass tube. The pH of the solution was adjusted to the desired value by adding a small amount of 0.01 M NaOH or 0.01 M HCl. The mixture was shaken at room temperature for 2 min on a Vortex shaker (Spinix). After 24 h the suspension was centrifuged at 3500 rpm for 20 min. Centrifugation prior to the measurement was performed to avoid potential interference from scattering particles in the UV–vis analysis. The supernatant was pipetted out and the unadsorbed RMPs measured directly by the UV–vis spectrophotometry at their characteristic values of λ_{max} which was 259 nm for 5′-AMP, 252 nm for guanosine 5′-monophosphate (5′-GMP), 272 nm for cytidine

https://doi.org/10.1017/S1473550415000348 Published online by Cambridge University Press

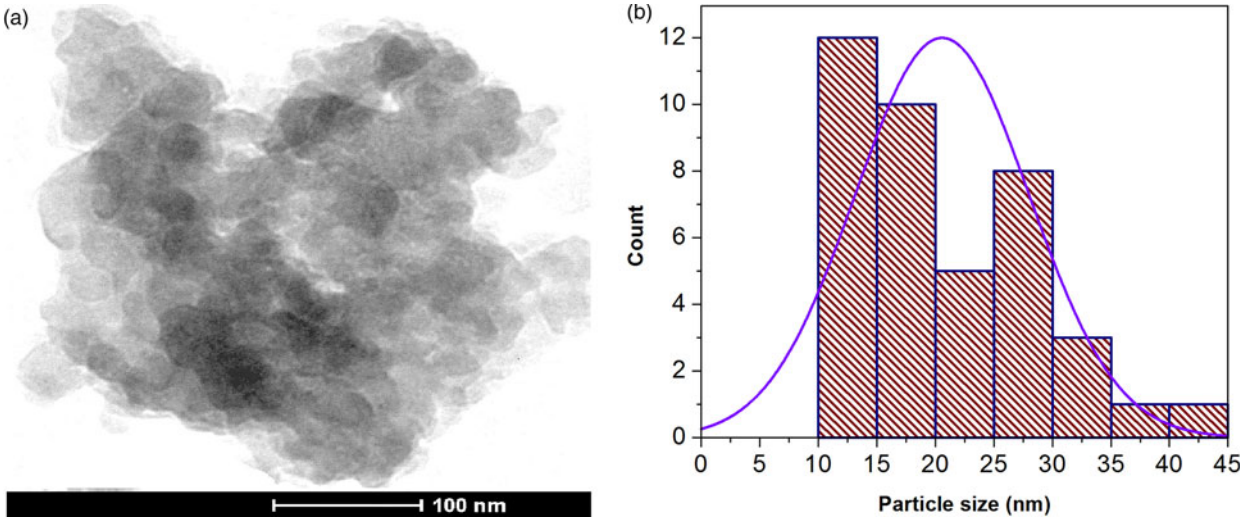

Fig. 1. (a) TEM image and (b) corresponding particle size distribution curve of PB.

5′-monophosphate (5′-CMP) and 262 nm for uridine 5′-monophosphate (5′-UMP). The adsorbed amount of RMPs at equilibrium, X_e (mg g^{-1}) was calculated by the following expression:

$$X_e = \frac{(C_i - C_{eq}) \times M \times V \times 1000}{m} \text{ mg}$$

where X_e is the amount (mg) of adsorbate adsorbed on 1 g of adsorbent; C_i and C_{eq} are the initial and equilibrium concentrations of RMP solution, respectively; V the volume of the adsorbate solution; M the molecular weight of the adsorbate; and m the amount (mg) of the adsorbent used.

The equilibrium concentration of ribose nucleotide and the amount adsorbed were used to obtain the adsorption isotherms. The solid residue was dried for 24 h and analysed with FT-IR, FE-SEM, XRD and Raman spectroscopy to know the nature of adsorption.

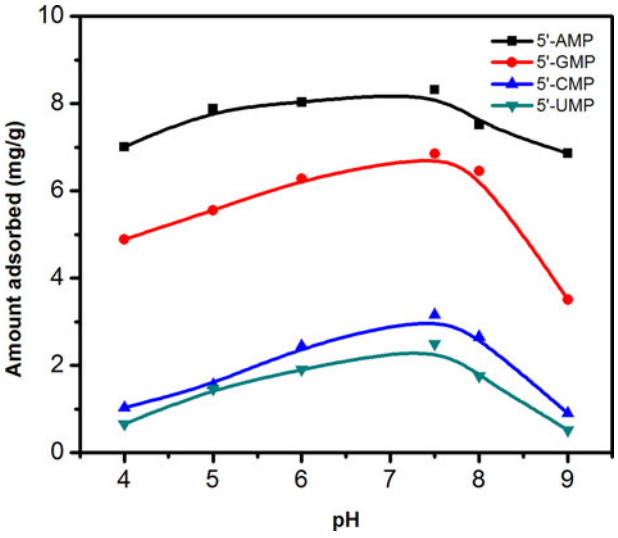

Fig. 2. Effect of pH on RMPs adsorption.

Results and discussion

Characterization of PB

Table S2 (supplementary section) shows the results obtained by CHNS and atomic absorption spectroscopy (AAS) analyses of PB nanoparticles where the amount of elements is given in weight per cent. The thermogravimetric analysis (TGA) profile of the PB is presented in Figure S1 (supplementary section). From the CHNS, AAS and TGA data, the molecular formula of PB was determined as $Fe_4[Fe(CN)_6]_3.15H_2O$. The UV–vis spectrum of PB is presented in Figure S2 (supplementary information). The spectrum of PB shows a broad band at 700 nm due to intervalent electron transfer from iron(II) to iron(III) in a polymeric sequence of PB.

The XRD pattern of the synthesized sample (Figure S3 in supplementary portion) exhibited characteristic peaks corresponding to PB (JCPDS file no. 73-0687) at 2θ values of 17.45 (200), 24.73 (220), 35.22 (400), 39.54 (420) and 43.60 (422). The pattern obtained is consistent with a face-centred cubic structure of PB with space group Fm3 m. The broad diffraction peaks in the spectrum are related to the nanosized particle with a crystallite size of 10.75 nm which has been calculated using the Debye–Scherrer equation.

$$D = \frac{0.89 \times \lambda}{\beta \times \cos\theta}$$

where D is the crystallite size, λ is the wavelength of the X-ray radiation (0.1540 nm for Cu-Kα radiation), β is the full-width at half-maximum and θ is the diffraction angle. The values of the lattice parameter 'a' are calculated from the most prominent peak in the XRD of PB using the formula $a = d\sqrt{h^2 + k^2 + l^2}$, where h, k and l are the miller indices of the crystal plane (200) and 'd' is the interplanar spacing (0.5076 nm) obtained by the XRD pattern. The lattice parameter 1.015 nm obtained is in good agreement with the reported value of 1.013 nm (Herren *et al.* 1980). The observed value of

https://doi.org/10.1017/S1473550415000348 Published online by Cambridge University Press

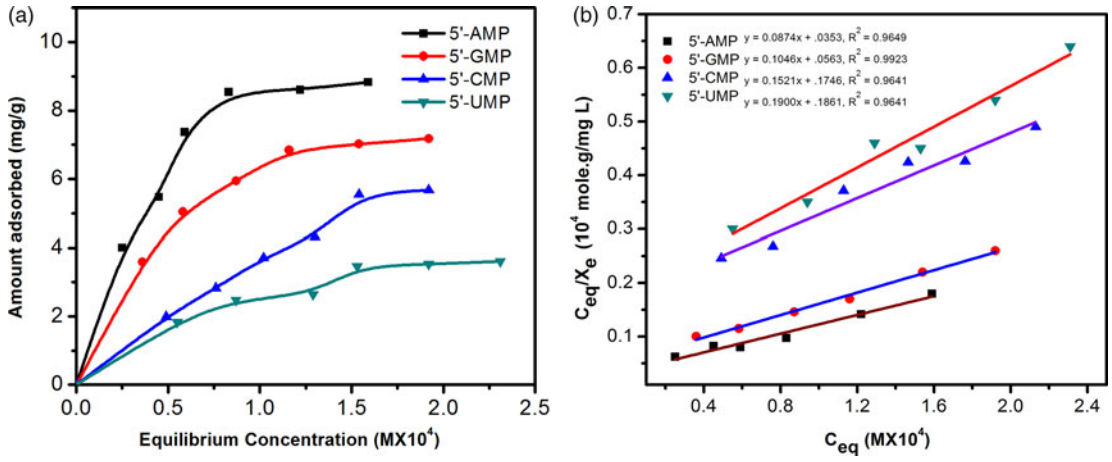

Fig. 3. (a) Adsorption isotherms and (b) Langmuir plots of RMPs on PB.

the crystallite size was also quite consistent with the TEM results. PB is aggregated in the form of particles in the diameter range of 10–20 nm. The particle size distribution plot also suggests that the average particle size of PB is in the range of 10–20 nm (Fig. 1(a) and (b)). The size of the PB particles prepared by us is in good agreement with the literature report (Gotoh *et al.* 2007).

Adsorption of RMPs on PB

Effect of contact time

The effect of the contact time on the adsorption of RMPs by PB is shown in Figure S4 (supplementary section), which demonstrated that the adsorption process was rapid at the initial stage of the contact period and gradually became constant. The availability of uncovered surface area and the active sites on the adsorbent account for the fast adsorption of RMPs at the initial stage of the adsorption process. As the optimum contact time was found to be 24 h, the equilibrium time for further study has been taken as 24 h to ensure the steady state.

Effect of adsorbent amount

To analyse the effect of the amount of adsorbent on the per cent adsorption of the RMPs, the studies were carried out by varying the amounts of adsorbents from 10 to 35 mg of PB at fixed RMP concentration (2.0×10^{-4} M). Figure S5 (supplementary information) demonstrated that the per cent adsorption of RMPs increased with increasing amounts of PB. The maximum adsorption capacity has been obtained at 25 mg of the adsorbent, after which increasing in adsorbent amount does not further increase the per cent adsorption and the amount adsorbed remain almost constant. Thus, all the investigations were carried out with a fixed amount of adsorbent of 25 mg.

Effect of pH

The pH is considered to be one of the most important factors influencing the adsorption process. It influences not only surface charge of the adsorbent, but also the dissociation equilibrium of the adsorbate in solution. To study the influence of pH on the adsorption capacity of PB for RMPs, experiments were performed at room temperature and an initial concentration of 2.0×10^{-4} M of RMPs using different initial pH values, in the range of 4.0–9.0. The results of RMP adsorption obtained at different solution pH values are shown in Fig. 2. In all cases, the maximum amount of RMPs was adsorbed at a pH value of about 7.5. The proton dissociation of the phosphate group in RMPs takes place with corresponding pk_{a1} and pk_{a2} values (Table S1). In the pH range 2–4, the RMPs are present in its monoanionic form. At pH higher than 4, the fractions of RMP^- gradually decrease by the removal of the hydrogen ion to form RMP^{2-}. The fractions of RMP^{2-} start to increase after pH 4 and reach its maximum values at around pH 8. Based upon this observation we performed the adsorption studies at pH 7.5 where electrostatic interaction may take place between positively charged surface of adsorbent and negatively charged phosphate moiety.

Adsorption isotherms

Equilibrium isotherms provide information about the adsorption mechanism, surface properties and the affinity of the adsorbent. The adsorption isotherm studies were conducted by varying the initial concentration of RMPs from 0.4×10^{-4} to 3.0×10^{-4} M, while the adsorbent mass (25 mg) was kept constant at pH 7.5 for 24 h. Figure 3(a) depicts the adsorption isotherms (X_e versus C_{eq}) and shows that the adsorption capacity increased with the increasing equilibrium concentration of RMP and eventually attained a constant value. The per cent binding for all the four RMPs corresponding to the saturation point of adsorption isotherm was calculated and listed in Table 1. The adsorption of RMPs on PB was found to be 53.1, 41.7, 25.8 and 24.0% for 5′-AMP, 5′-GMP, 5′-CMP and 5′-UMP, respectively. 5′-AMP, 5′-GMP, 5′-CMP and 5′-UMP RMPs have been reported to be adsorbed on Na^+-montmorillonite clay as 19, 19, 15 and 11%, respectively. In case of Cu^{2+}-monmorillonite clay, the per cent binging for adenine and uridine mononucleotides was found to be 63 and 33%, respectively (Ferris *et al.* 1989). Although the surface area

https://doi.org/10.1017/S1473550415000348 Published online by Cambridge University Press

Table 1. *Per cent binding and Langmuir isotherms parameters of RMPs on the surface of PB*

Ribose nucleotides	Per cent binding	Langmuir parameters		
		X_m (mg g^{-1})	$K_L \times 10^{-4}$ (l mol^{-1})	R^2
5′-AMP	53.1	11.5	2.5	0.96
5′-GMP	41.7	9.6	1.9	0.99
5′-CMP	25.8	6.6	0.87	0.94
5′-UMP	24.0	5.3	1.02	0.96

Table 2. *Adsorption kinetics constants for 5′-AMP adsorption on PB*

Kinetic model	Values
Pseudo-first order	
k_1 (L h^{-1})	0.20
X_e (mg g^{-1})	6.37 mg g^{-1}
R^2	0.89
Pseudo-second order	
k_2 (g mg^{-1} h)	0.08
X_e (mg g^{-1})	9.67 mg g^{-1}
R^2	0.99

(242 m^2 g^{-1}) of PB is lower as compared with montmorillonite (750 m^2 g^{-1}) but still it acts as a good adsorbent for RMPs. Due to the mesoporous nature of PB, it is proposed that PB might have interacted with the biomonomers to concentrate them from their dilute aqueous solutions in primeval seas.

In order to obtain information on the properties and mechanism of the interaction, the adsorption data obtained were fitted to the Langmuir adsorption model. The basic assumption of this model is to consider the maximum adsorption capacity consisting of a monolayer adsorption and homogenous distribution of adsorption energy over the adsorbent surface. Further, the model also assumes that there are no interactions between the adsorbed molecules. The conventional Langmuir equation is as follows (Langmuir 1916; Kobya 2003):

$$X_e = \frac{X_m \times K_L \times C_{eq}}{1 + K_L \times C_{eq}}$$

where X_e is the equilibrium adsorption capacity (mg g^{-1}); X_m the maximum adsorption capacity (mg g^{-1}); and K_L the Langmuir adsorption constant (l mol^{-1}).

Langmuir equation can be expressed in a linear form which is given as,

$$\frac{C_{eq}}{X_e} = \frac{C_{eq}}{X_m} + \frac{1}{X_m K_L}$$

A straight line plot (Fig. 3(b)) was obtained upon plotting C_{eq}/X_e versus C_{eq} and thus the Langmuir adsorption isotherm was found to be obeyed. The linearity of the Langmuir isotherms indicates the formation of a monolayer of RMPs on PB surface. The Langmuir adsorption constants (K_L and X_m) were calculated for all the RMPs from the intercept and slope of the corresponding plots. The Langmuir adsorption

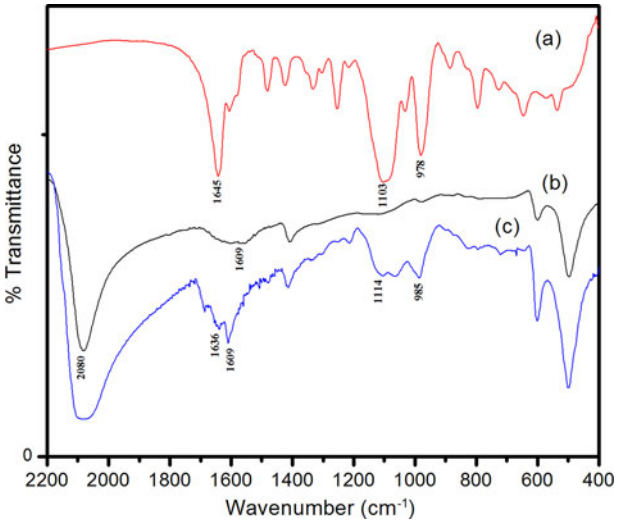

Fig. 4. A typical FT-IR spectra of (a) 5′-AMP, (b) PB and (c) 5′-AMP-PB adduct.

constants and correlation coefficient (R^2) values are summarized in Table 1.

Adsorption kinetics

Two kinetic models, the pseudo-first and pseudo-second-order models were used to examine the kinetics of the adsorption process of the 5′-AMP. The obtained adsorption data were fit in these two models. The differential form of pseudo-first-order equation (Ho & McKay 1998) can be represented as

$$\frac{dX_t}{dt} = k_1(X_e - X_t)$$

where X_e is the amount adsorbed (mg g^{-1}) at the equilibrium; X_t the amount adsorbed (mg g^{-1}) at time t; and k_1 is the pseudo-first-order rate constant (h^{-1}).

Integrating the above equation under the boundary conditions from $t = 0$ to $t = t$ and $X_t = 0$ to $X_t = X_e$, a simplified linear form of the pseudo-first-order rate equation can be expressed as

$$\ln(X_e - X_t) = \ln X_e - k_1 t$$

A plot of $\ln(X_e - X_t)$ versus t gives a straight line. The slope and the intercept of the plot were used to find out the values of k_1 and X_e.

The linear form of the pseudo-second-order rate equation (Ho & McKay 2000) can be represented as,

$$\frac{t}{X_t} = \frac{1}{(k_2 X_e^2)} + \frac{t}{X_e}$$

where k_2 denotes the rate constant (g mg^{-1} h) for pseudo-second-order kinetic model. The observed values of pseudo-first and pseudo-second-order model parameters for 5′-AMP are shown in Table 2. The correlation coefficient (R^2) data for the pseudo-second-order case is relatively higher than for the pseudo-first-order kinetics model. This indicates that the adsorption of RMPs could be best interpreted by a pseudo-second-order kinetics model.

https://doi.org/10.1017/S1473550415000348 Published online by Cambridge University Press

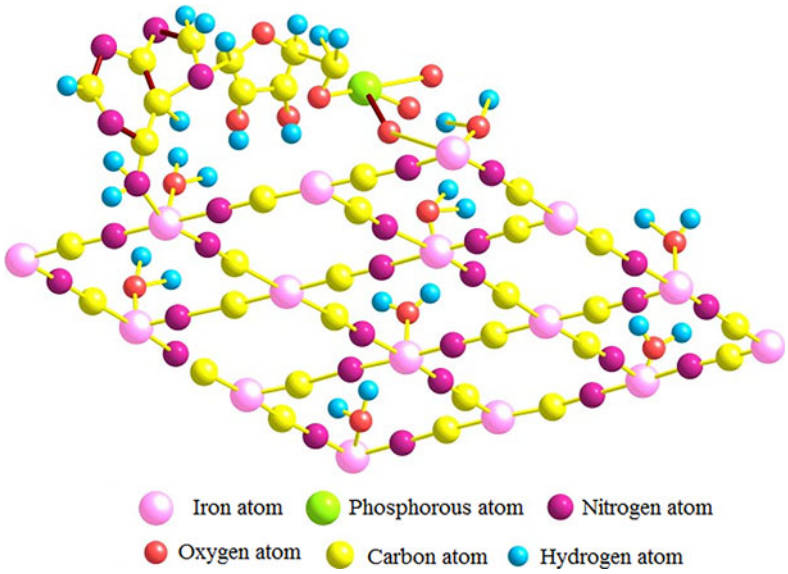

Fig. 5. A probable structure of 5′-AMP–PB adduct.

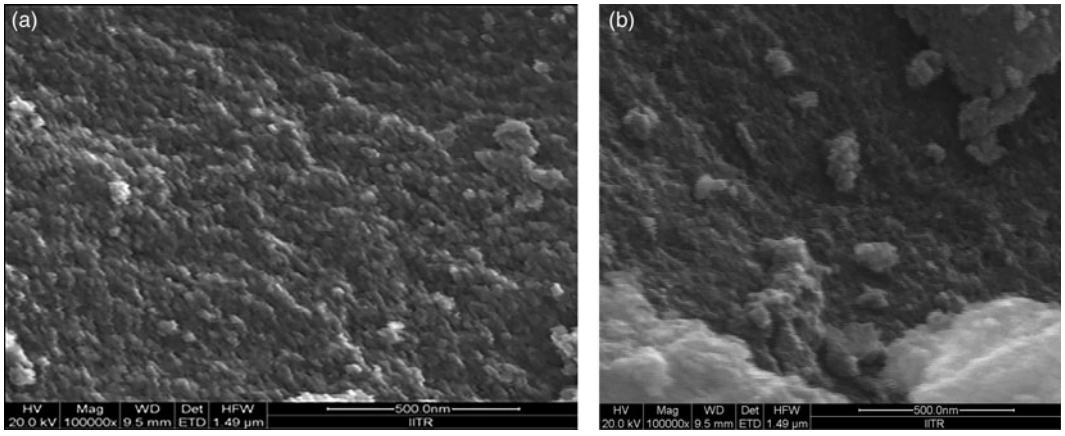

Fig. 6. FE-SEM images of PB and (b) 5′-AMP–PB adduct.

The change of Gibbs free energy (ΔG) is an important parameter to evaluate for the spontaneity of a reaction. As reported in the literature ΔG related to the adsorption process can be calculated using the following equations (Wu 2007):

$$\Delta G = -\mathrm{RT}\ \ln K_c$$

$$K_c = \frac{(C_i - C_e)}{C_e}$$

where K_c is the equilibrium constant, T is the absolute temperature and R is the universal gas constant. The calculated value of ΔG in case of 5′-AMP adsorption on PB was found to be −0.85 kJ mol^{-1}. The negative value of ΔG suggest that the adsorption of RMPs on PB surface was spontaneous and feasible. The values of free energy change in case of physisorption and chemisorption are reported to be in the ranges of (−20 to 0 kJ mol^{-1}) and (−80 to −400 kJ mol^{-1}), respectively (Mahmoodi *et al.* 2011). The value obtained for ΔG (−0.85 kJ mol^{-1}) in our study suggests that physisorption is the primary mechanism for RMP adsorption on the PB surface.

Fourier transform infrared spectra

The FT-IR spectra of PB, 5′-AMP and 5′-AMP–PB adduct are illustrated in Fig. 4. The main peaks of the PB were as the following; sharp peak at 2080 cm^{-1} corresponded to the C–N stretching mode of Fe–CN bond and 1609 cm^{-1} corresponding to the O–H bending of interstitial water molecule, respectively. Peak at 601 and 498 cm^{-1} were attributed with the Fe–CN bending. For the 5′-AMP molecule, the peak at 1645 cm^{-1} was assigned with NH_2 deformation (Tajmir-Riahi & Theophanides 1983). The peaks centred at 1103 and 978 cm^{-1} were assigned to the $\vartheta(PO_3^{2-})$ antisymmetric and $\vartheta(PO_3^{2-})$ symmetric, respectively. The interaction of RMPs on the surface of PB alters the characteristics peaks of RMPs which are summarized in Table S3 (supplementary data). Upon interaction with PB, the ϑNH_2 peak is shifted to 1636

https://doi.org/10.1017/S1473550415000348 Published online by Cambridge University Press

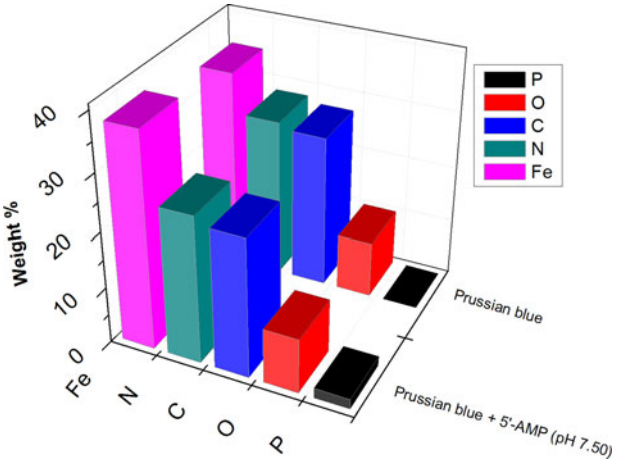

Fig. 7. EDX weight per cent of P, O, C, N and Fe in adsorbent (PB) and 5′-AMP–PB adduct at pH 7.5.

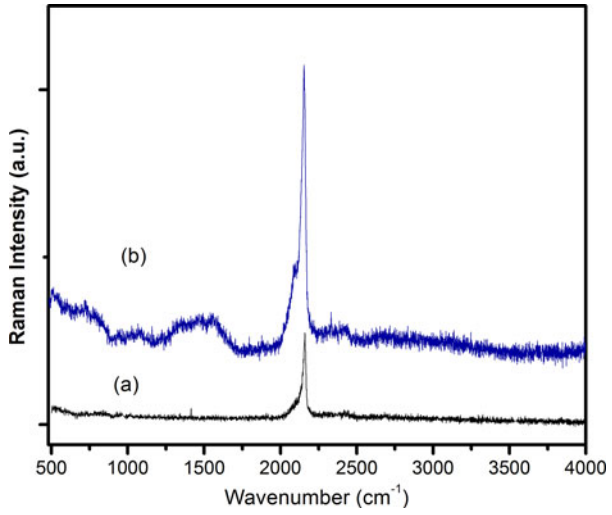

Fig. 8. Raman spectra of (a) PB and (b) 5′-AMP–PB adduct.

cm^{-1}, which showed the involvement of NH_2 groups in the adsorption process. The strong peaks of $\vartheta(PO_3^{2-})$ antisymmetric and $\vartheta(PO_3^{2-})$ symmetric shifted to the frequencies of 1114 and 985 cm^{-1}, strongly suggesting that the interaction is taking place through the phosphate moiety of RMPs with PB. No notable change in characteristic frequencies of PB after adsorption suggests that RMPs molecule do not enter into the coordination sphere of PB by replacing cyanide ions. A possible interaction scheme between PB and 5′-AMP is shown in Fig. 5. The structure reveals that the Fe(III) atom binds with the phosphate moiety and with the NH_2 group of AMP, therefore changes occur in the frequency of N–H bending and phosphate stretching mode.

Field-emission scanning electron microscopy

FE-SEM was employed to observe the attachment of ribose nucleotides on the PB surface. The SEM images showed in Fig. 6(a) and (b) demonstrate that the surface morphology of PB and 5′-AMP–PB adduct are different. PB composed of

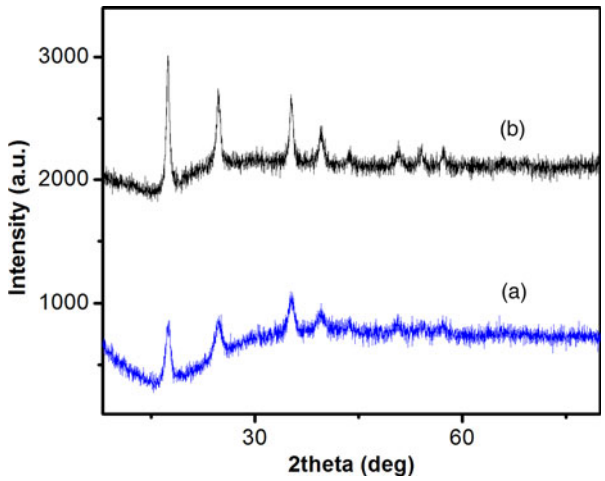

Fig. 9. XRD patterns of (a) PB and (b) 5′-AMP–PB adduct.

globular-shaped particles has a tendency to aggregate. The 5′-AMP molecules were attached on the surface of PB as shown in Fig. 6(b). In the EDX plot (Fig. 7) presence of phosphorous in AMP–PB adduct in addition to elements present in PB also confirm the adsorption of 5′-AMP on the surface of PB.

Raman spectroscopy

In Fig. 8, the Raman spectra of PB and PB–AMP adduct are shown. The Raman spectra of PB show a strong vibrational band at 2135 cm^{-1} which is caused by the stretching vibration of carbon nitrogen triple bond group of PB, while the Raman spectra of PB–AMP adduct showed some additional peaks other than the cyanide stretching band. The presence of the adsorbed AMP is clearly evident by the presence of the Raman bands at 1015 and 1590 cm^{-1} which corresponds to the phosphate stretching and in-plane symmetric NH_2 scissor mode of AMP, respectively (Kundu *et al.* 2009).

XRD analysis

Adsorption process may change the molecular and crystalline structures of the adsorbent. So to better understand the adsorption phenomenon XRD patterns of the adsorbent before and after the adsorption of 5′-AMP have been investigated and are shown in Fig. 9. The XRD patterns reveal that after the adsorption of 5′-AMP on the PB surface the major XRD peaks of PB have been shifted. The peaks at $2\theta = 17.45°$, 24.73° and 35.22° are shifted to $2\theta = 17.75°$, 25.01° and 35.85°. Thus shifting and increase in the peak intensity confirm the adsorption of RMPs on the PB surface.

Textural characteristics

In Fig. 10, the nitrogen adsorption–desorption isotherms of PB and PB–AMP adduct are shown. These isotherms are nearly related to the type IV isotherm, which is the characteristic of mesoporous materials (Brunauer *et al.* 1940). The BET surface areas for the PB and PB–AMP adduct are 242.0 and 146.0 $m^2\ g^{-1}$, respectively. The considerable decrease in the BET surface

https://doi.org/10.1017/S1473550415000348 Published online by Cambridge University Press

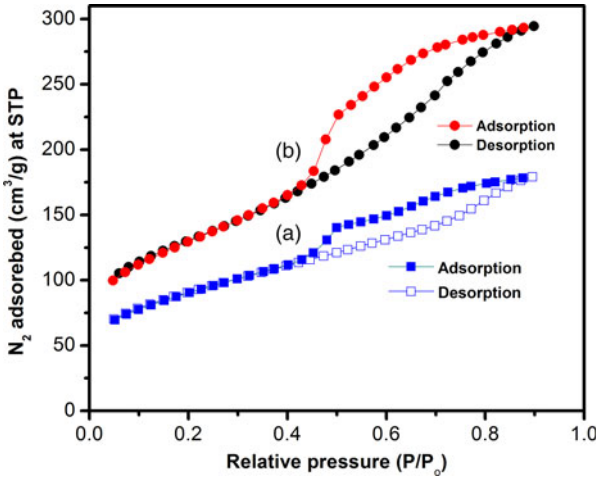

Fig. 10. N_2 adsorption–desorption isotherm of (a) 5′-AMP + PB adduct and (b) PB.

area of PB suggests that a considerable amount of RMPs have been adsorbed to the PB surface. Pore volume in PB and PB–AMP adduct was also calculated and compared to confirm the adsorption of RMPs on PB surface. The values of the pore volume for PB and PB–AMP adduct are 0.323 and 0.162 $cm^3\ g^{-1}$, respectively, as determined using the Barrett-Joyner-Halenda (BJH) pore size distribution method (Barrett *et al.* 1951). The significant decrease in the pore volume of PB further indicates the adsorption of RMPs onto the PB surface.

Conclusion

Adsorption of RMPs on the PB surface has been studied for better understanding the adsorption mechanism. Adsorption of RMPs was confirmed by FT-IR, Raman spectroscopy, FE-SEM and XRD techniques. Gibbs free energy value was calculated for 5′-AMP adsorption which was found to be negative (-0.85 kJ mol^{-1}), suggesting that the adsorption process of RMP on PB was spontaneous in nature. A typical adsorption kinetics of 5′-AMP fitted a pseudo-second-order model better than pseudo-first-order one. The results obtained in our study have relevance for prebiotic chemistry scenarios and more generally for biomedical applications involving adsorption of biomolecules.

Supplementary material

Supplementary materials of this paper is available at http://dx.doi.org/10.1017/S1473550415000348

Acknowledgment

One of the authors (RS) is grateful to MHRD for a fellowship.

References

Ali, S.R. & Kamaluddin, (2007). Interaction of ribonucleotides with hexacyanocobaltate(III): a possible role in chemical evolution. *Orig. Life Evol. Biosph.* **37**, 225–234.

Ali, S.R., Ahmad, J. & Kamaluddin (2004). Interaction of ribose nucleotides with metal ferrocyanides and its relevance in chemical evolution. *Colloids Surf. A* **236**, 165–169.

Arora, A.K. & Kamaluddin (2007). Interaction of ribose nucleotides with zinc oxide and relevance in chemical evolution. *Colloids Surf. A: Physicochem. Eng. Asp.* **298**, 186–191.

Arora, A.K. & Kamaluddin, (2009). Role of metal oxides in chemical evolution: interaction of ribose nucleotides with alumina. *Astrobiology* **9**(2), 165–171.

Arora, A.K., Tomar, V., Aarti, N., Venkateswararao, K.T. & Kamaluddin (2007). Haematite-water system on Mars and its possible role in chemical evolution. *Int. J. Astrobiol.* **6**, 267–271.

Arrhenius, T., Arrhenius, G. & Paplawsky, W. (1994). Archean geochemistry of formaldehyde and cyanogen and the oligomerozation of cyanohydrin. *Orig. Life Evol. Biosph.* **24**, 1–17.

Barrett, E.P., Joyner, L.G. & Halenda, P.P. (1951). The determination of pore volume and area distributions in porous substances. I. Computations from nitrogen isotherms. *J. Am. Chem. Soc.* **73**(1), 373–380.

Bau, J.P.T. *et al.* (2012). Adsorption of adenine and thymine on Zeolites: FT-IR and EPR spectroscopy and X-ray diffractometry and SEM studies. *Orig. Life Evol. Biosph.* **42**, 19–29.

Bermejo, M.R., Menor-Salvan, C., Osuna-Esteban, S. & Veintemillas-Verdaguer, S. (2007). The effects of ferrous and other ions on the abiotic formation of biomolecules using aqueous aerosols and spark discharges. *Orig. Life Evol. Biosph.* **37**, 50–521.

Bernal, J.D. (1951). *The Physical Basis of Life.* Routledge and Kegan Paul, London.

Brunauer, S., Emmett, P.H. & Teller, E. (1938). Adsorption of gases in multimolecular layers. *J. Am. Chem. Soc.* **60**(2), 309–319.

Brunauer, S., Deming, L. S., Deming, W. E. & Teller, E. (1940). On a theory of the van der Waals adsorption of gases. *J. A. Chem. Soc.* **62**(7), 1723–1732.

Cai, P., Huang, Q., Zhang, X. & Chen, H. (2006). Adsorption of DNA on clay minerals and various colloidal particles from an Alfisol. *Soil Biol. Biochem.* **38**, 471–476.

Carneiro, C.E.A., Berndt, G., Souza, T.G.D., Souza, C.M.D.D., Paesano, A., Costa, A.C.S.D., Mauro, E.D., Santana, H.D. & Zaia, D.A.M. (2011). Adsorption of adenine, cytosine, thymine and uracil on sulfide-modified Montmorillonite: FT-IR, Mossbauer and EPR spectroscopy and X-ray diffractometry studies. *Orig. Life Evol. Biosph.* **41**, 453–468.

Cleaves, H.J., Jonsson, C.M., Jonsson, C.L., Sverjensky, D.A. & Hazen, R. M. (2010). Adsorption of nucleic acid components on rutile (TiO_2) surfaces. *Astrobiology* **10**, 311–323.

Ferris, J.P. & Hagan, W.J. (1986). The adsorption and reaction of adenine-nucleotides on montmorillonite. *Orig. Life Evol. Biosph.* **17**, 69–84.

Ferris, J.P., Ertem, G. & Agarwal, V.K. (1989). The adsorption of nucleotides and polynucleotides on montmorillonite clay. *Orig. Life Evol. Biosph.* **19**, 153–164.

Feuillie, C., Daniel, I., Michot, L.J. & Pedreira-Segade, U. (2013). Adsorption of nucleotides onto Fe–Mg–Al rich swelling clays. *Geochim. Cosmochim. Acta* **120**, 97–108.

Franchi, M., Bramanti, E., Bonzi, L.M., Orioli, P.L., Vettori, C. & Gallori, E. (1999). Clay-nucleic acid complexes: characteristics and implications for the preservation of genetic material in primeval habitats. *Orig. Life Evol. Biosph.* **29**, 297–315.

Franchi, M., Ferris, J.P. & Gallori, E. (2003). Cations as mediators of the adsorption of nucleic acids on clay surfaces in prebiotic environments. *Orig. Life Evol. Biosph.* **33**, 1–16.

Georgelin, T., Jaber, M., Onfroy, T., Hargrove, A.A., Costa-Torro, F. & Lambert, J.F. (2013). Inorganic phosphate and nucleotides on silica

surfaces: condensation, dismutation, and phosphorylation. *J. Phys. Chem. C* **117**(24), 12579–12590.

Gibson, C.H., Wickramasinghe, N.C. & Schild, R.E. (2010). First life in primordial-planet oceans: the biological big bang. *J. Cosmol.* **11**, 3490–3499.

Gotoh, A. *et al*. (2007). Simple synthesis of three primary colour nanoparticles inks of Prussian blue and its analogues. *Nanotechnology* **18**, 355609 (6 pp).

Hashizume, H. & Theng, B.K.G. (2007). Adenine, adenosine, ribose and 5′-AMP adsorption to allophane. *Clays Clay Miner.* **55**, 599–605.

Hashizume, H., Van der Gaast, S. & Theng, B.K.G. (2010). Adsorption of adenine, cytosine, uracil, ribose, and phosphate by Mg-exchanged montmorillonite. *Clays Clay Miner.* **45**, 469–475.

Herren, F., Fischer, P., Ludi, A. & Hälg, W. (1980). Neutron diffraction study of Prussian blue, $Fe_4[Fe(CN)_6]_3.xH_2O$. Location of water molecules and long-range magnetic order. *Inorg. Chem.* **19**(4), 956–959.

Ho, Y.S. & McKay, G. (1998). A comparison of chemisorption kinetic models applied to pollutant removal on various sorbents. *Process Saf. Environ. Protect.* **76**, 332–340.

Ho, Y.S. & McKay, G. (2000). The kinetics of sorption of divalent metal ions onto sphagnum moss peat. *Water Res.* **34**, 735–742.

Holm, N.G., Ertem, G. & Ferris, J.P. (1993). The binding and reactions of nucleotides and polynucleotides on iron-oxide hydroxide polymorphs. *Orig. Life Evol. Biosph.* **23**, 195–215.

Keefe, A.D. & Miller, S.L. (1996). Was ferrocyanide a prebiotic reagent? *Orig. Life Evol. Biosph.* **26**, 111–129.

Kobya, M. (2003). Adsorption, kinetics and equilibrium studies of Cr(VI) by Hazelnut shell activated carbon. *Adsorp. Sci. Technol.* **22**, 51–64.

Kumar, A. & Kamaluddin, (2013). Possible role of metal(II) octacyanomolybdate(IV) in chemical evolution: interaction with ribose nucleotides. *Orig. Life Evol. Biosph.* **43**, 1–17.

Kundu, J., Neumann, O., Janesko, B.G., Zhang, D., Lal, S., Barhoumi, A., Seuseria, G.E. & Halas, N.J. (2009). Adenine and adenosine monophosphate (AMP)−gold binding interactions studied by surface-enhanced Raman and infrared spectroscopies. *J. Phys.Chem.* **C113**(32), 14390–14397.

Langmuir, I. (1916). The constitution and fundamental properties of solids and liquids. *J. Am. Chem. Soc.* **38**, 2221–2295.

Lohrmann, R. & Orgel, L.E. (1971). Urea–inorganic phosphate mixtures as prebiotic phosphorylating agents. *Science* **171**(3970), 490–494.

Mahmoodi, N.M., Hayati, B., Arami, M. & Lan, C. (2011). Adsorption of textile dyes on Pine Cone from colored waste water: kinetic, equilibrium and thermodynamic studies. *Desalination* **268**, 117–125.

Powner, M.W., Gerland, B. & Sutherland, J.D. (2009). Synthesis of activated pyrimidine ribonucleotides in prebiotically plausible conditions. *Nature* **459**, 239–242.

Sciascia, L., Liveri, M.L.T. & Merli, M. (2011). Kinetic and equilibrium studies for the adsorption of acid nucleic bases onto K10 montmorillonite. *Appl. Clay Sci.* **53**, 657–668.

Szostak, J.W. (2009). Origins of life: systems chemistry on early Earth. *Nature* **459**(7244), 171–172.

Tajmir-Riahi, H.A. & Theophanides, T. (1983). Adenosine-5′-monophosphate complexes of Pt (II) and Mg (II) metal ions. Synthesis, FT-IR spectra and structural studies. *Inorg. Chim. Acta* **80**, 183–190.

Wu, C.H. (2007). Adsorption of reactive dye onto carbon nanotubes: equilibrium, kinetics and thermodynamics. *J. Hazard Mater.* **144**, 93–100.

Yamagata, Y., Watanabe, H., Saitoh, M. & Namba, T. (1991). Volcanic production of polyphosphates and its relevance to prebiotic evolution. *Nature* **352**, 516–519.